

## Conformational studies of bottle-brush polymers absorbed on a flat solid surface

Hsiao-Ping Hsu,<sup>1</sup> Wolfgang Paul,<sup>2,a)</sup> and Kurt Binder<sup>1</sup>

<sup>1</sup>*Institut für Physik, Johannes Gutenberg-Universität Mainz, Staudinger Weg 7, D-55099 Mainz, Germany*

<sup>2</sup>*Theoretische Physik, Martin Luther Universität Halle-Wittenberg, von Seckendorffplatz 1, 06120 Halle, Germany*

(Received 13 July 2010; accepted 9 September 2010; published online 7 October 2010)

The adsorption of a bottle-brush polymer end-grafted with one chain end of its backbone to a flat substrate surface is studied by Monte Carlo simulation of a coarse-grained model, that previously has been characterized in the bulk, assuming a dilute solution under good solvent conditions. Applying the bond fluctuation model on the simple cubic lattice, we vary the backbone chain length  $N_b$  from  $N_b=67$  to  $N_b=259$  effective monomeric units, the side chain length  $N$  from  $N=6$  to  $N=48$ , and set the grafting density to  $\sigma=1$ , i.e., parameters that correspond well to the experimentally accessible range. When the adsorption energy strength  $\epsilon$  is varied, we find that the adsorption transition (which becomes well-defined in the limit  $N_b \rightarrow \infty$ , for arbitrary finite  $N$ ) roughly occurs at the same value  $\epsilon_c$  as for ordinary linear chains ( $N=0$ ), at least within our statistical errors. Mean square end-to-end distances and gyration radii of the side chains are obtained, as well as the monomer density profile in the direction perpendicular to the adsorbing surface. We show that for longer side chains the adsorption of bottle-brushes is a two-step process, the decrease of the perpendicular linear dimension of side chains with adsorption energy strength can even be nonmonotonic. Also, the behavior of the static structure factor  $S(q)$  is analyzed, evidence for a quasi-two-dimensional scaling is presented, and consequences for the interpretation of experiments are discussed. © 2010 American Institute of Physics. [doi:10.1063/1.3495478]

### I. INTRODUCTION

Macromolecules with a comblike chemical architecture, where flexible side chains are densely grafted to a (also flexible) polymer acting as “backbone” have found abiding current interest (see, e.g., the recent reviews<sup>1–4</sup>). These so-called “bottle-brush polymers” exhibit an interesting competition due to the steric repulsion between the side chains and the configurational entropy of the backbone: varying the grafting density of the side chains and their length, the effective stiffness of these cylindrical brushes can be controlled over a wide range. Since the overall conformation of the bottle-brush polymer is sensitive to external stimuli such as solvent quality, pH value and ionic strength of the solution, temperature, or electromagnetic fields, various possible applications of these bottle-brush polymers have been discussed (actuators, sensors, building blocks of new nanostructures, or templates for producing metallic nanowires<sup>5–9</sup>). A fascinating aspect is also the importance of biomolecules with bottle-brush architecture, such as proteoglycans<sup>10</sup> (polyelectrolytes consisting of a protein backbone and carbohydrate side chains, performing biological functions from cell signaling and cell surface protection to joint lubrication<sup>11,12</sup>). Of course, under many circumstances these functions of bottle-brushes occur when they are attached to a substrate surface (e.g., a cell membrane in a biological context or an inorganic flat solid surface for nanotechnological applications, including also special surface coatings<sup>13</sup>). Bottle-brush molecules attached

to surfaces are also of particular interest since additional experimental tools become available to study their structure (e.g., one can directly visualize their large-scale conformation by scanning force microscopy,<sup>3,14,15</sup> or one can use atomic force microscopes to measure force versus extension curves<sup>16</sup>). Thus, while rich information on the structure of bottle-brush polymers at surfaces already is available,<sup>3</sup> it is not so clear which of these features are intrinsic properties of these complex macromolecules and which features are only induced by their adsorption to the substrate. We recall that basic aspects of bottle-brush polymers in dilute solution away from any constraining surfaces are still incompletely understood (e.g., the relation between the persistence length of these macromolecules and their microscopic characteristics such as side chain and backbone chain lengths  $N$  and  $N_b$  has been controversial; see, e.g., Refs. 17–19). There are already some indications from theoretical work<sup>20,21</sup> that strongly adsorbed bottle-brushes exhibit properties different from the bulk.

Thus, the present paper intends to contribute to a clarification of this problem by presenting a comprehensive computer simulation study of (large) bottle-brush polymers near surfaces over the full range extending from a repulsive surface (applying only the constraint that one backbone chain end is grafted to this surface) through the region of the adsorption transition, where the overall conformation of the macromolecule changes from a three-dimensional “mushroom” to a quasi-two-dimensional “pancake” to the strongly adsorbed almost two-dimensional case. Using side chain

<sup>a)</sup>Electronic mail: wolfgang.paul@physik.uni-halle.de.

lengths up to  $N=48$ , we ensure that statistical concepts of theoretical polymer physics<sup>22</sup> start to become applicable,<sup>23</sup> and we also note that our range of side chain lengths can be nicely mapped to experiments.<sup>19</sup> While the adsorption transition of flexible linear chains has been studied extensively by various theoretical methods,<sup>24–32</sup> the present work is the first one to present large-scale simulations on the adsorption of bottle-brush polymers. Clearly, the interplay of the conformational changes due to adsorption with the chain stiffness (tunable via the side chain length variation) is of particular interest.<sup>33</sup>

The plan of this paper is as follows. Section II describes the model and the simulation techniques, while Sec. III presents the numerical results. Section IV gives a summary and an outlook on both pertinent experimental work and on open questions.

## II. MODEL AND SIMULATION TECHNIQUE

The bond fluctuation model on the simple cubic lattice<sup>34–37</sup> has been extended in a previous work to simulate bottle-brush polymers in dilute solution under good solvent conditions.<sup>19,38</sup> In the present paper, we extend these studies to bottle-brush polymers tethered with one chain end of their backbone to a flat impenetrable surface, which is chosen to be the  $xy$ -plane ( $z=0$ ) of the lattice. Besides the excluded volume interactions between the monomers of the side chains and/or the backbone chain, and the infinitely repulsive interaction between monomers and the grafting surfaces (which prevents that monomers can occur with  $z$ -coordinates  $z<0$  in the system), we also consider the effect of an additional attractive short range interaction  $\epsilon$  between the grafting surface and the monomers of the bottle-brush polymer. Recall that in the bond fluctuation model, each effective monomer blocks all eight sites at the corners of an elementary cube of the lattice from further occupation. Thus, an energy  $\epsilon$  is won if four sites of such a cube are in plane  $z=0$ , while the remaining four sites of the cube then have to be in the adjacent plane  $z=1$  (note that we use the lattice spacing as the unit of length).

The bond vectors connecting two adjacent monomers along a chain are chosen from the set  $\{[2,0,0], [2,1,0], [2,1,1], [2,2,1], [3,0,0], \text{ and } [3,1,0]\}$ , including also all possible rotations, reflections, and reversions of these bond vectors. We use the same set of bond vectors, irrespective of whether we consider side chains of the bottle-brush or the backbone chain. Note that this model is one of the standard models used for Monte Carlo simulation of macromolecular systems, many physical properties of polymers are rather well accounted for, and very efficient simulation algorithms can be formulated for this model.<sup>39</sup>

The chemical architecture of a bottle-brush polymer is arranged such that at a backbone monomer that acts as a grafting site, one side chain is anchored, and the chemical distance (i.e., difference in the consecutive labels of the backbone monomers) is the inverse of the grafting density,  $1/\sigma$ . Thus, only integer numbers  $1/\sigma$  are possible, and side chains are anchored at regular chemical distances. Note that both next to the first grafting site and next to the last grafting

site of the backbone, we add one extra backbone monomer. Thus, if we have  $n_c$  side chains, the total number of monomers in the backbone is  $N_b = [(n_c - 1)/\sigma + 1] + 2$ , and the total number of monomers in the bottle-brush then is  $N_{\text{tot}} = N_b + n_c N$ , when  $N$  denotes the number of monomers per side chain. Now, we also require that one of the two extra monomers at a chain end of the backbone is attached to the adsorbing surface at  $z=0$ , and hence our simulation deals with a “bottle-brush mushroom” (recall that an isolated polymer chain<sup>24</sup> end-grafted to a planar surface traditionally is called a “polymer mushroom,” and we extend this nomenclature to bottle-brushes). In the present work, only  $\sigma=1$  is considered.

The initial configuration of the bottle-brush polymer is constructed by assuming that the structures of the backbone chain and of the side chains are both rodlike. Namely, the backbone is oriented in the direction along the  $+z$ -direction, setting all bond vectors between monomers equal to  $\vec{r}=3\hat{z}$ , where  $\hat{z}$  is a unit vector along the  $z$ -axis. The bond vectors between monomers on each side chain are chosen randomly from one of the allowed bond vectors in the  $x$ - $y$  plane. This initial configuration, of course, is very far from equilibrium and needs to be carefully relaxed toward equilibrium in the first part of the Monte Carlo run.

In order to speed up the dynamics of the model, we do not move the monomers from their previous positions to only one of the six nearest neighbor sites of the monomer, as is traditionally done, but allow attempts to move a monomer to one of the 26 sites surrounding the current position of the monomer. This “L26 move” allows bonds to cross each other and has been shown to yield a significant speedup of the algorithm in comparison with the standard “L6” move.<sup>39</sup> In addition to the local moves, the pivot algorithm<sup>40</sup> is employed in the following ways. (a) A monomer on the backbone is chosen randomly and the part of the bottle-brush polymer containing the free end of the backbone is exposed to a trial move by randomly choosing one operation from the 48 symmetry operations of the lattice (no change, rotations by  $90^\circ$  and  $180^\circ$  angles, reflections, and inversions). Of course, the trial configuration is accepted as a new configuration only if it does not violate any excluded volume constraints and if it passes the Metropolis acceptance test (where the change in adsorption energy enters). The same is true for the attempted “L26” moves, of course. (b) A monomer is chosen randomly from the monomers on all side chains, and

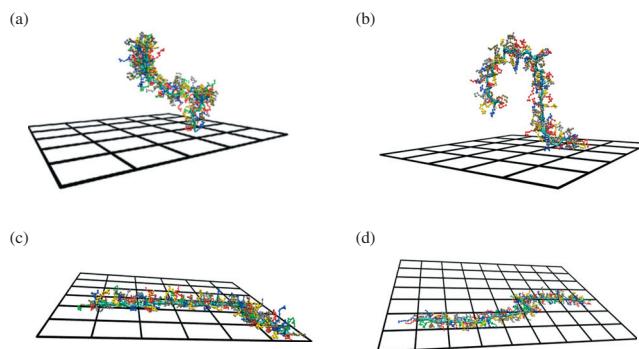


FIG. 1. Snapshots of typical configurations of bottle-brush polymers for backbone chain length  $N_b=131$  and side chain length  $N=12$  and four choices of adsorption energy  $\epsilon$ , namely, (a)  $\epsilon=0$ , (b) 1.0, (c) 1.5, and (d) 2.0.



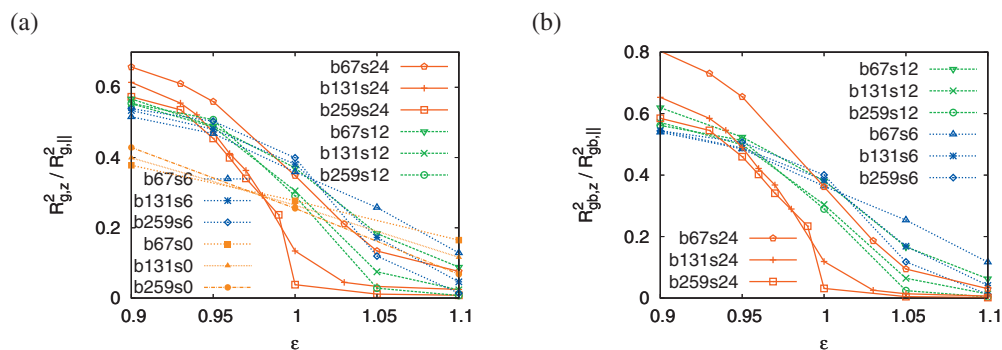


FIG. 4. Same figures as shown in Figs. 2(b) and 3(a) but for the data in the range  $0.9 < \epsilon < 1.1$ . For  $N=12$  and  $N=24$ , the backbone chain length  $N_b=67$  is too short, so the expected scaling behavior (which requires an intersection of the curves at  $\epsilon_c$ ) is not yet seen.

ponent  $\phi$  (the “crossover exponent”<sup>26</sup>) such that the fraction of monomer-surface contacts  $N_s/N_b$  behaves as (in the limit  $N_b \rightarrow \infty$ )<sup>26</sup>

$$\frac{N_s}{N_b} \propto \begin{cases} \frac{1}{N_b} (1 - \epsilon/\epsilon_c)^{-1}, & \epsilon < \epsilon_c \\ N_b^{\phi-1}, & \epsilon = \epsilon_c \\ (\epsilon/\epsilon_c - 1)^{1/\phi-1}, & \epsilon > \epsilon_c. \end{cases} \quad (1)$$

Despite a lot of effort (see Refs. 28–32 and references therein), the value of the (universal) exponent  $\phi$  is not yet very precisely known, some estimates being compatible with  $\phi=0.50 \pm 0.02$ .<sup>29,30</sup> However, the most recent estimate from Monte Carlo simulations of the bond fluctuation model yielded<sup>32</sup>  $\phi=0.59$ , a value close to the early estimate<sup>26</sup>  $\phi=0.58$ . This adsorption transition also shows up in the chain linear dimensions, of course. For  $\epsilon \leq \epsilon_c$ , all linear dimensions are of the same order,<sup>26,28</sup>

$$R_{g,z}^2 \propto R_{g,||}^2 \propto N_b^{2\nu}, \quad \nu \approx 0.588. \quad (2)$$

For  $\epsilon > \epsilon_c$ , the perpendicular component of the gyration radius (related to the thickness of the “pancake” configuration) remains finite,<sup>26</sup>

$$R_{g,z}^2 \propto (\epsilon/\epsilon_c - 1)^{-2\nu/\phi}, \quad (3)$$

while the parallel component exhibits a scaling compatible with two-dimensional self-avoiding walks,<sup>26</sup>

$$R_{g,||}^2 \propto (\epsilon/\epsilon_c - 1)^{2(\nu_2 - \nu)/\phi} N_b^{2\nu_2}, \quad \nu_2 = 3/4. \quad (4)$$

Hence, when one plots the ratio  $R_{g,z}^2/R_{g,||}^2$  versus  $\epsilon$  for several finite large values of  $N_b$ , one should see a family of curves, which exhibit an intersection point for  $\epsilon = \epsilon_c$ .

Motivated by Eqs. (1), (3), and (4), we plot the fraction of monomer-surface contacts  $N_s/N_{\text{tot}}$  versus  $\epsilon$  [Fig. 2(a)],  $N_{\text{tot}}$  being the total number of effective monomers in the bottle-brush polymer, as well as the ratio  $R_{g,z}^2/R_{g,||}^2$  [Fig. 2(b)]. An inspection of these “raw data” (Figs. 2 and 3) already indicates that the adsorption transition occurs near  $\epsilon_c(N) \approx 1.00 \pm 0.05$  (see Fig. 4, a close view of the ratio  $R_{g,z}^2/R_{g,||}^2$  in the vicinity of  $\epsilon=1$ ); if  $\epsilon_c(N)$  depends at all on side chain length  $N$ , the dependence is rather weak. However, it is remarkable that  $N_s/N_{\text{tot}}$  increases for  $\epsilon > \epsilon_c(N)$  clearly much faster for the linear chains ( $N=0$ ) than for the bottle-brush polymers;  $N_s/N_{\text{tot}}$  seems to converge to a limiting function for large  $N$  that is independent of  $N$ . In contrast, the ratio  $R_{g,z}^2/R_{g,||}^2$  varies more steeply the larger  $N$ , and there is no universal behavior; in particular, in the nonadsorbing regime,  $R_{g,z}^2/R_{g,||}^2$  increases monotonically with  $N$ . This behavior is plausible since the longer the side chains are the more the excluded volume interaction with the planar substrate surface is felt.

Of course, it would be desirable to extract more precise estimates of  $\epsilon_c(N)$  from a scaling analysis of the data, similar to the scaling analysis done in Refs. 26, 29, 31, and 32. Unfortunately, as explained in the Appendix, no significant gain in accuracy in comparison with the simple intersection

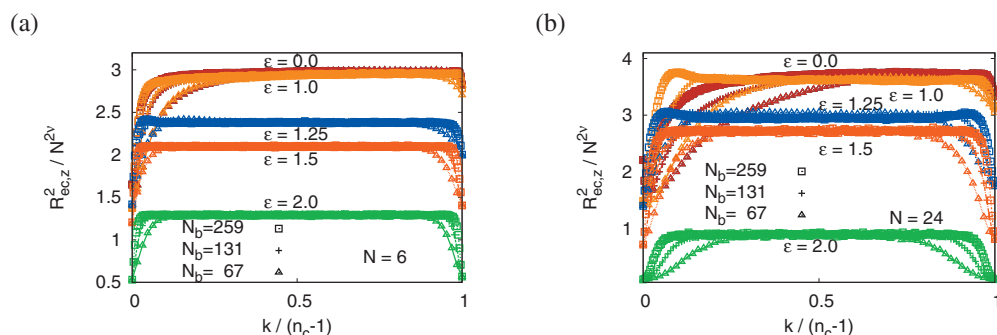


FIG. 5. Rescaled mean square end-to-end distance of the side chains, perpendicular to the surface,  $R_{ec,z}^2/N^{2\nu}$ , vs the normalized position  $k/(n_c-1)$  in the coordinate system along the backbone (the  $n_c$  side chains are labeled  $k=0, 1, \dots, n_c-1$ , the side chain with  $k=0$  is next to the grafted backbone monomer, while the side chain with  $k=n_c-1$  is next to the backbone free end). Five choices of adsorption energies  $\epsilon=0, 1.0, 1.25, 1.5$ , and  $2.0$  are included, as indicated, as well as three choices of the backbone chain lengths  $N_b=67, 131$ , and  $259$ , respectively. Case (a) refers to  $N=6$ , and case (b) refers to  $N=24$ .

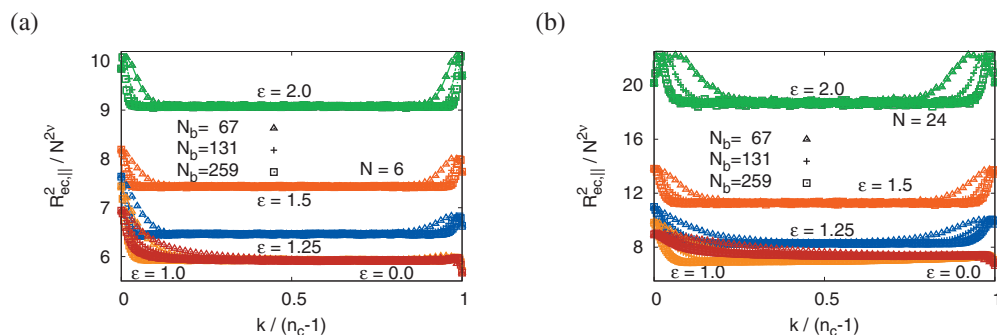


FIG. 6. Same as Fig. 5, but for the component parallel to the surface,  $R_{ec,||}^2/N^{2\nu}$ , plotted vs  $k/(n_c-1)$ .

method in Fig. 2(b) could be gotten. An obvious question with respect to the adsorption transition of bottle-brush polymers is the clarification whether the behavior of the side chains and of the backbone is fully analogous, or whether some characteristic differences occur. Thus, Fig. 3 disentangles in both the fraction of adsorbed monomers and in the ratio  $R_{g,z}^2/R_{g,||}^2$  the contributions of the backbone from the contributions of the side chains. One sees remarkable differences between the behavior of the side chains and the backbone; while the ratio  $R_{gc,z}^2/R_{gc,||}^2$  is essentially constant for  $\epsilon \leq \epsilon_c$  and then decreases only rather gradually (almost linearly), the ratio  $R_{gb,z}^2/R_{gb,||}^2$  shows most of its decrease before  $\epsilon_c \approx 1.0$  is reached. On the other hand, for large  $N$ , a significant rise of  $N_{sb}/N_b$  only starts at about  $\epsilon \approx 1.2 > \epsilon_c$ . Some aspects of this behavior can be attributed to the fact that in the adsorption of bottle-brushes, it easily happens that the monomer density in the layer adjacent to the adsorbing wall gets rather high; thus, there is not enough empty space in this layer to allow for the adsorption of all the side chain monomers.

Since some of the side chains near the backbone chain end that is grafted to the substrate surface necessarily are rather close to the adsorbing surface, while this is not true for the side chains in the vicinity of its free ends, it also is interesting to resolve the side chain properties as a function of their position along the backbone (Fig. 5). One can see that the linear dimensions of the side chains near to the grafted backbone chain end are strongly reduced for nonadsorbed chains, while an analogous effect near the free backbone end is much smaller. No such asymmetry can occur for free bottle-brush polymers in bulk solution, of course, since there both backbone chain ends are strictly equivalent. It is

remarkable, however, that this asymmetry effect vanishes almost completely when the bottle-brush polymer gets adsorbed; then, also the free chain end of the backbone is close to the surface, and it does not matter whether it actually would be grafted or not. A similar asymmetry is found, however, when one considers the mean square end-to-end distance of the side chains parallel to the surface (Fig. 6); of course, then the magnitude of  $R_{ec,||}^2/N^{2\nu}$  strongly increases with  $\epsilon$ , unlike  $R_{ec,z}^2/N^{2\nu}$ , due to the tendency of the adsorbed polymers to form “pancake” conformations, cf. Eqs. (3) and (4), and therefore, these ratios systematically increase with increasing  $N$ .

Similar observations can be made when one studies the mean square gyration radius components (Figs. 7 and 8). Thus, if one would normalize the data for  $R_{ec,||}^2$  with  $N^{2\nu_2}$  with  $\nu_2=3/4$  instead of  $N^{2\nu}$  with  $\nu=0.588$ , as done in Fig. 6, one finds plateau values for  $\epsilon=2.0$  in the center of the bottle-brush ( $0.2 < k/(n_c-1) < 0.8$ ) at about 5.1 for  $N=6$  and at about 6.8 for  $N=24$ . These values are of the same order as seen in Fig. 6 for  $\epsilon \leq 1.0$ , where the side chains still take the configuration of three-dimensional coils. Of course, side chain lengths  $N \leq 48$ , as studied here, are too short to reveal the asymptotic behavior  $R_{ec,||}^2 \propto N^{2\nu_2}$  in the regime  $\epsilon > \epsilon_c$  clearly.

A rather unexpected feature, however, emerges when we examine the variation of the radii with  $\epsilon$  (Fig. 9). The side chain linear dimensions are almost independent of  $N_b$  for  $\epsilon < 1$ . The adsorption process for  $\epsilon > 1$ , however, seems to be an  $N$ -dependent two-step process: first a rather rapid decrease of  $R_{gc,z}^2$  (and a rather rapid increase of  $R_{gc,||}^2$ ) occurs, and the behavior for all three values of  $N$  is rather similar;

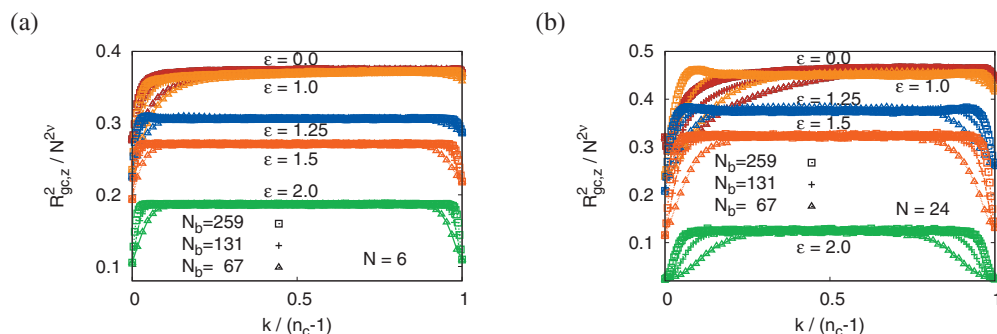


FIG. 7. Same as Fig. 5, but for the rescaled mean square gyration radius of the side chains, perpendicular to the surface,  $R_{gc,z}^2/N^{2\nu}$ , for (a)  $N=6$  and (b)  $N=24$ .

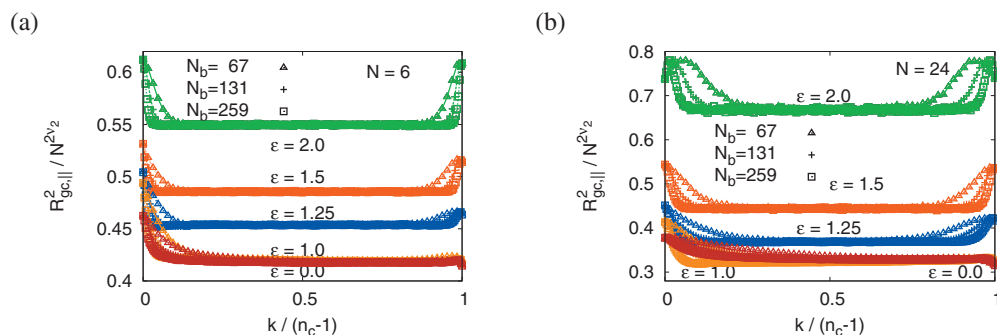


FIG. 8. Same as Fig. 5, but for  $R_{gc,||}^2/N^{2\nu_2}$ , plotted vs  $k/(n_c-1)$ . Note that by the normalization with  $N^{2\nu_2}$  rather than  $N^{2\nu}$ , the shown ratios approach a finite limit for  $N \rightarrow \infty$ , unlike in Fig. 6.

then, near  $\epsilon \approx 1.25$ , the behavior changes, and the further variation depends distinctly on  $N$  and for  $R_{gc,z}^2$  and  $N=24$  even is nonmonotonic. Near  $\epsilon \approx 1.7$ , the three sets of curves intersect each other. We speculate that for  $\epsilon < 1.25$ , the adsorption is controlled by the side chains near the grafted end of the backbone, while for  $\epsilon > 1.25$ , it is controlled by all the side chains and the backbone, but clearly this point needs further study. Of course,  $R_{gc,z}^2$  can be considered as a measure of the thickness of the “pancake.”

Alternative information on this thickness can be obtained when one simply studies the monomer density profile  $P(z)$ , which again can also be resolved distinguishing contributions from the backbone only, from the side chains only, or even from the free chain ends of the side chains only (Figs. 10–14).

While for  $N=6$  the monomer distribution of the bottle-brush as a whole for the nonadsorbed bottle-brush mushroom and the distribution of the backbone and the side chain monomers are very similar to each other and similar to corresponding data for simple nonadsorbed polymer mushrooms, the distribution gets a more complicated shape the longer the side chain length  $N$  becomes. The strong shift of the maximum of all distributions with increasing  $N$  to larger  $z$  can clearly be attributed to the increasing backbone stiffness and the corresponding increase of the linear dimensions of the bottle-brush. When now the adsorption energy is switched on, the distributions show little change for  $\epsilon \leq 0.5$  (not shown), while near the adsorption transition, a profound change of the character of the distribution has occurred (Fig. 12): all distributions now exhibit a second maximum near the

surface, for large enough  $N$ , and also the main maximum occurs now much closer to the adsorbing surface (but its position  $z_{\max}$  strongly increases with  $N$ , presumably because the bottle-brush needs to avoid “crowding” of monomers near the adsorbing surface). In the adsorbed regime (Figs. 13 and 14), one observes layering type oscillations near the wall, similar to the behavior of off-lattice models for fluids close to hard walls. While the backbone monomers still have a pronounced maximum in  $P(z)$  away from the surface, Fig. 13(b), the corresponding results for the side chain monomers do not show this maximum any more. This observation corroborates our interpretation of the nonmonotonic variation of  $R_{gc,z}^2$  in Fig. 9, namely, that adsorption occurs in two steps—first, the adsorption of the monomers near the grafted end of the backbone takes place, while the adsorption transition of the rest of the bottle-brush is not yet completed at  $\epsilon = 1.25$  for the side chain lengths  $N$  studied here. For  $\epsilon = 1.5$ , on the other hand, all profiles show only very little dependence on the side chain length (Fig. 14). The lengths of still nonadsorbed “tails” and “loops”<sup>27</sup> then are rather short, and therefore the side chain length no longer is important.

From the profiles, one can easily estimate the average thickness  $\langle z \rangle$  defined as  $\langle z \rangle = \int_0^\infty z P(z) dz / \int_0^\infty P(z) dz$  and study its dependence on  $\epsilon$  (Fig. 15). Again, the two-step character of adsorption for long enough side chains ( $N=24$ ) is very clearly seen.

As a final point of this study, we address the scattering function  $S(q)$  where the orientation of the wave vector  $\vec{q}$  has been averaged over. Hence,

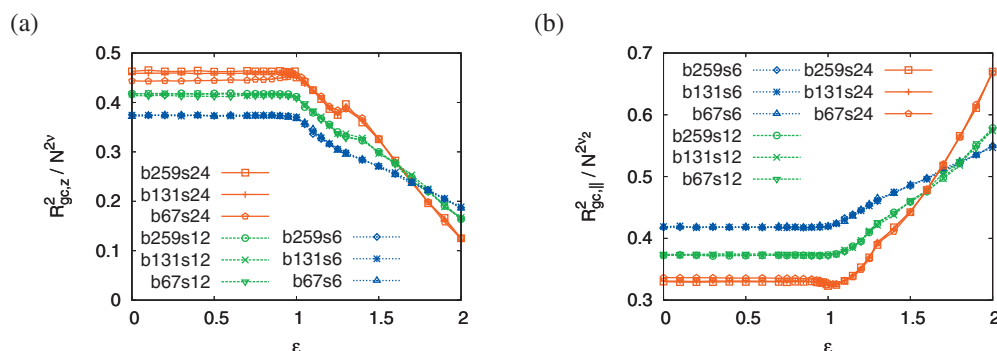


FIG. 9. Rescaled mean square gyration radius (a)  $R_{gc,z}^2/N^{2\nu}$  and (b)  $R_{gc,||}^2/N^{2\nu_2}$  plotted vs  $\epsilon$ , including data for three different backbone chain lengths  $N_b = 67, 131, \text{ and } 259$  as well as three different side chain lengths  $N=6, 12, \text{ and } 24$  (the various combinations of  $N_b$  and  $N$  are indicated in the figure as  $bN_b sN$ , respectively). Note that these data, unlike in Figs. 7 and 8, are averages along the backbone.

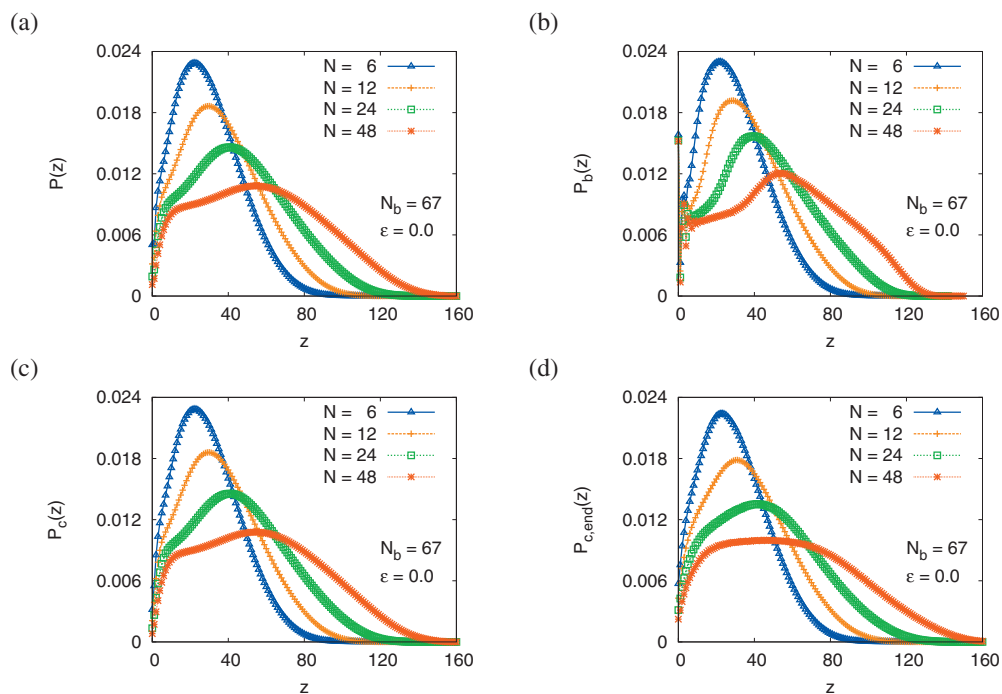


FIG. 10. Monomer density profiles of the bottle-brush polymers  $P(z)$  as a function of the distance  $z$  from the surface for backbone chain length  $N_b=67$  at the nonadsorbing case ( $\epsilon=0.0$ ) and four side chain lengths  $N=6, 12, 24,$  and  $48$ . Case (a) refers to all monomers of the bottle-brush, case (b) includes monomers of the backbone only, case (c) includes only the side chains, and case (d) includes only the free ends of the side chains.

$$S(q) = \frac{1}{\mathcal{N}^2} \left\langle \sum_{j=0}^{\mathcal{N}} \sum_{k=0}^{\mathcal{N}} \exp[i\vec{q} \cdot (\vec{r}_j - \vec{r}_k)] \right\rangle, \quad (5)$$

where  $\mathcal{N}$  is the total number of monomers, from which the scattering is considered, and the average  $\langle \dots \rangle$  includes both a statistical average over the conformations of the bottle-brush and a spherical average over the direction of  $\vec{q}$ . A distinctive advantage of the simulation is that the scattering from the

total bottle-brush, the scattering only from the backbone, or only from the side chains are easily accessible.

Figure 16 correspondingly compares data for  $S(q)$  considering the total scattering from all the monomers of the bottle-brush, comparing data for four choices of  $N$  and three choices of  $N_b$ , as indicated, and including data for both  $\epsilon = 0.0$  and  $\epsilon = 2.0$ . While the data for  $\epsilon = 0.0$  closely resemble the scattering function of isolated bottle-brush polymers in

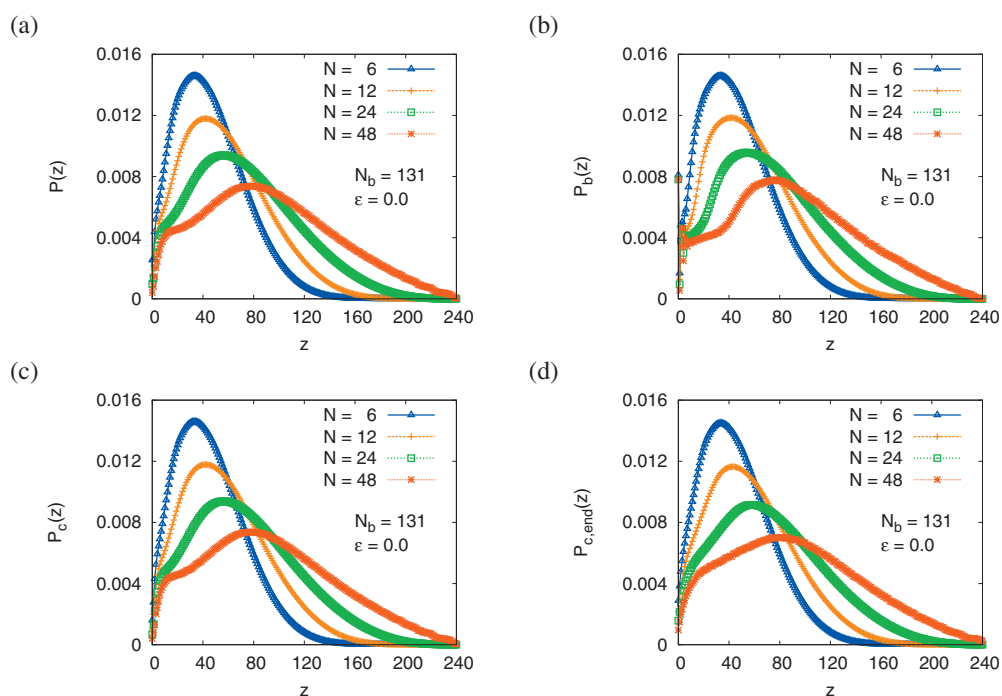
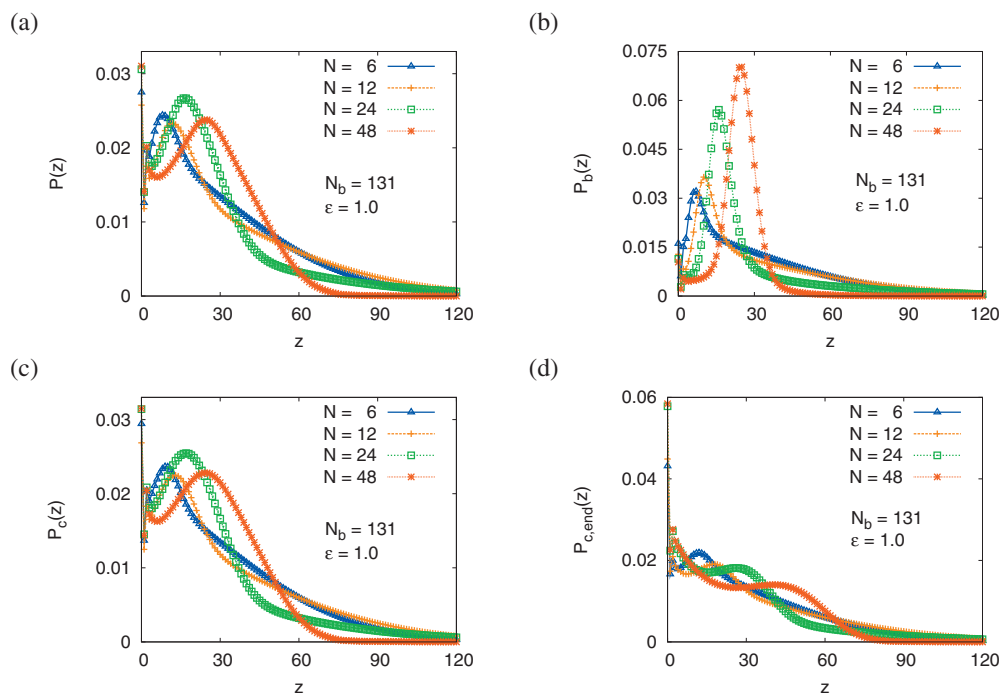


FIG. 11. Same as in Fig. 10 but for  $N_b=131$  and  $\epsilon=0.0$ .

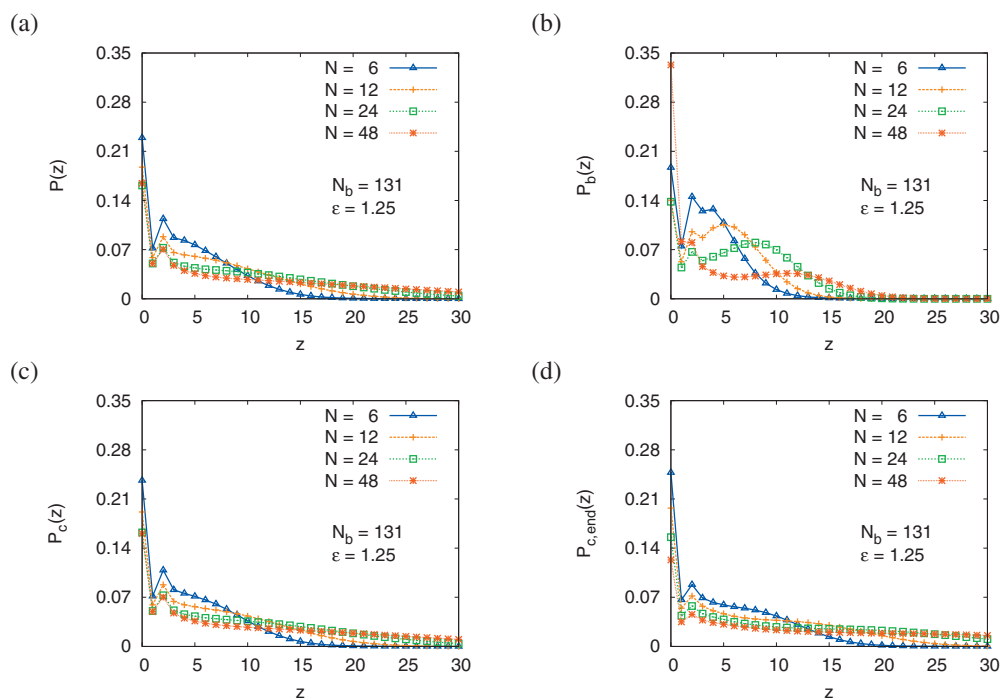
FIG. 12. Same as Fig. 10 but for  $N_b=131$  and  $\epsilon=1.0$ .

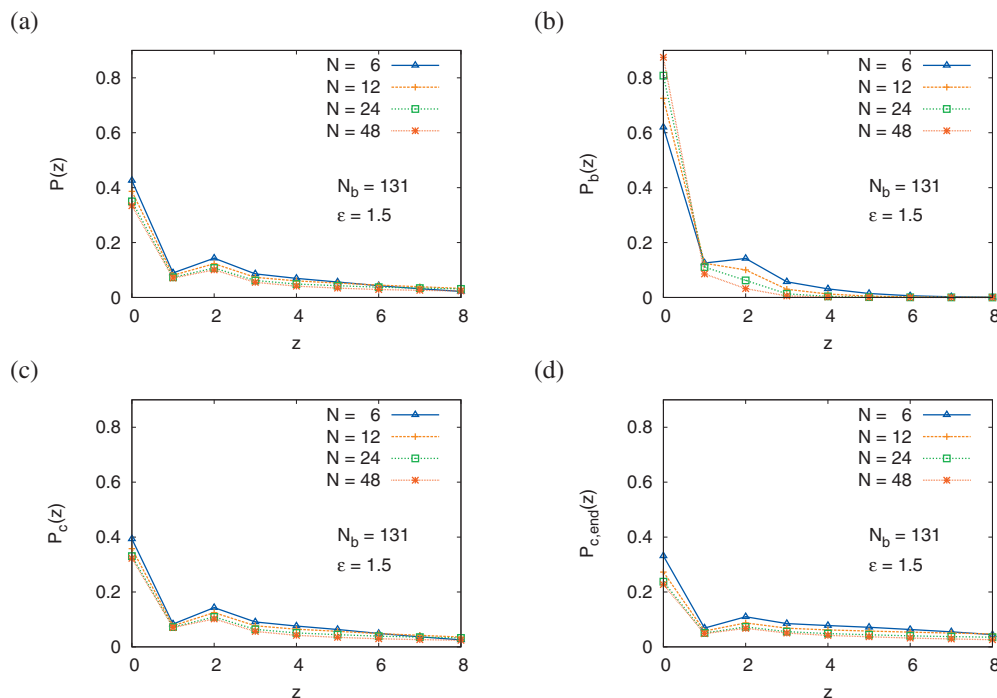
dilute bulk solution, as studied previously, revealing a law  $q^{-1/\nu}$  for small  $N$  and intermediate  $q$  and a rodlike behavior  $q^{-1}$  for large  $q$ , for the strongly adsorbed case ( $\epsilon=2.0$ ) for large  $q$ , the rodlike behavior is not seen for  $N=24$  and  $N=48$ ; rather, one finds in the decade  $0.1 \leq q \leq 1.0$  a behavior proportional to  $q^{-1/\nu_2} = q^{-4/3}$ . The side chains in the strongly adsorbed case behave like two-dimensional self-avoiding walks; since there are more monomers that occur in the side chains than in the backbone, the rodlike characteristics of the latter are only revealed when one focuses on the scattering

from the backbone only (Fig. 17). Then, one can clearly see two crossovers:  $S_b(q) \approx N_b(1 - q^2 \langle R_{g,b}^2 \rangle / 3)$  at small  $q$  of order  $\langle R_{g,b}^2 \rangle^{-1}$  crosses over to  $q^{-4/3}$  in  $d=2$  and to  $q^{-1/0.588}$  in  $d=3$  dimensions, while near  $q \approx 0.1$ , a crossover to  $S_b(q) \propto q^{-1}$  occurs both for adsorbed and for nonadsorbed bottle-brushes.

#### IV. SUMMARY

In this paper, a Monte Carlo simulation study of the adsorption of bottle-brush mushrooms (i.e., bottle-brush

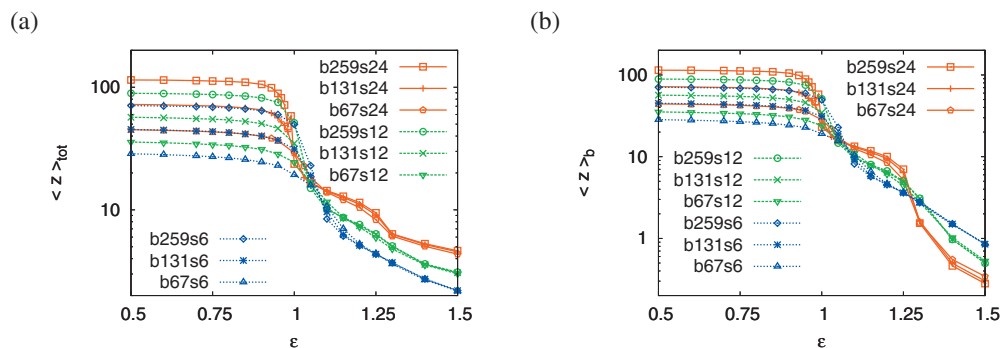
FIG. 13. Same as Fig. 10, but for  $N_b=131$  and  $\epsilon=1.25$ .

FIG. 14. Same as Fig. 10, but for  $N_b=131$  and  $\epsilon=1.50$ .

polymers with a backbone chain end-grafted to a flat structureless impenetrable surface) has been presented using the bond fluctuation model and assuming very good solvent conditions. The same range of backbone chain lengths ( $N_b \leq 259$ ) and side chain lengths ( $N \leq 48$ ) as used in a previous study of the same model in dilute solution in the bulk<sup>19</sup> has been used since evidence has been presented that this range is fully appropriate to allow a comparison with experiment.<sup>19</sup> Every backbone monomer carries one side chain.

Both the backbone chain and the side chains are assumed to be fully flexible, and a short range attractive energy  $\epsilon$  (putting temperature  $k_B T=1$  throughout) is assumed that attracts both monomers of the side chains and of the backbone to the surface in the same way. We show that near  $\epsilon_c(N)=1$ , the mushrooms cross over from a three-dimensional configuration (for  $\epsilon < 1$ ) to the adsorbed, quasi-two-dimensional configuration for  $\epsilon > 1$ . These transitions occur roughly at the same value of  $\epsilon_c(N)$  irrespective of  $N$ , but the latter has a pronounced effect deeper in the adsorbed region, where chain linear dimensions reveal a two-step ad-

sorption process (Figs. 9 and 15). We tentatively associate the first step of the adsorption (near  $\epsilon_c$ ) to the side chains near the grafted end of the backbone, while the backbone as a whole, for  $\epsilon$  not much larger than  $\epsilon_c$ , exhibits only a very small fraction  $N_{s,b}/N_b$  of adsorbed monomers [Fig. 3(c)]. Thus, most of the backbone monomers still occur in the tail or in rather long loops stretching away from the adsorbing surface. Only at somewhat larger values of  $\epsilon$  (namely, for  $\epsilon \approx 1.2$  in our case), the “trains”<sup>27</sup> of consecutively adsorbed backbone monomers get longer and more frequent, and the tail and the loops get correspondingly shorter. This behavior must cause an interesting interplay with the behavior of the side chains: a side chain grafted to a backbone monomer that is part of an adsorbed train behaves basically like a small mushroom, and hence such a side chain gets easily adsorbed. However, side chains grafted to a backbone monomer that belongs to the tail or to a large loop cannot yet get adsorbed easily simply because typically, the grafting site of this side chain is not close enough to the adsorbing surface. However, when  $\epsilon$  increases and the loops in the backbone would get

FIG. 15. Plot of  $\langle z \rangle$  (note the logarithmic scale) vs  $\epsilon$  for various choices of  $N_b$  and  $N$  (labeled as  $bN_b s N$  in the figure). Case (a) refers to all monomers of the bottle-brush; case (b) refers to backbone monomers only.

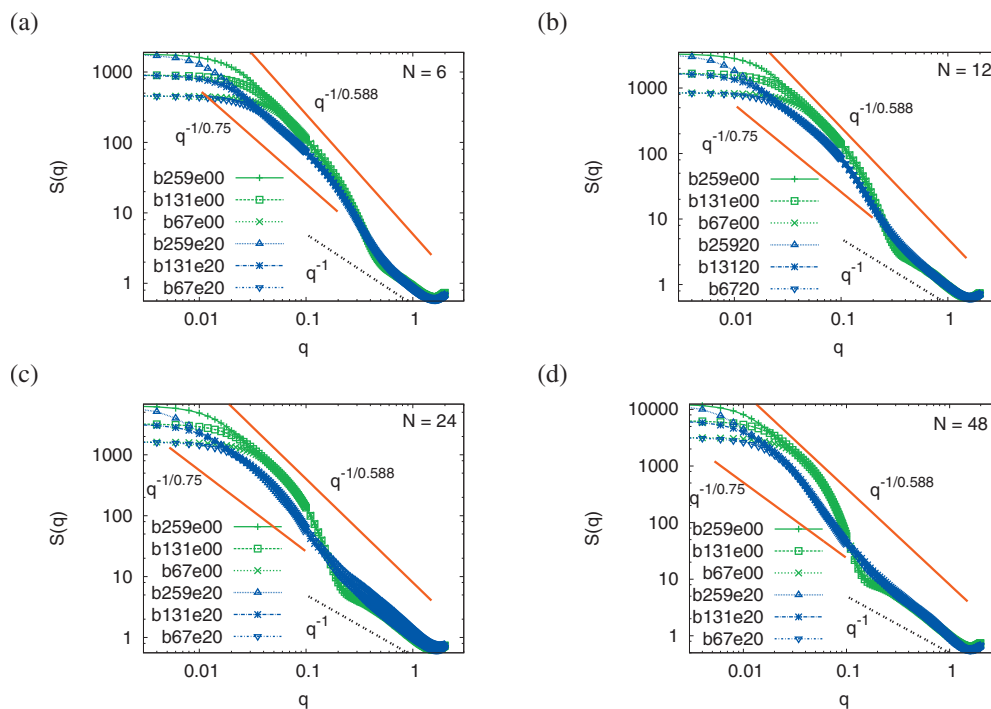


FIG. 16. Log-log plot of the scattering function  $S(q)$  of the whole bottle-brush polymers vs wave number  $q$  for side chain lengths (a)  $N=6$ , (b)  $N=12$ , (c)  $N=24$ , and (d)  $N=48$ . Three choices of backbone chain lengths  $N_b=67$ , 131, and 259 are included. Data for  $\epsilon=0.0$  are denoted as  $bN_b e00$ , while data for  $\epsilon=2.0$  are denoted as  $bN_b e20$ . Straight lines indicate the power laws for rods ( $q^{-1}$ ), three-dimensional coils ( $q^{-1/\nu}$  with  $\nu=0.588$ ), and two-dimensional coils ( $q^{-1/\nu_2}$ ,  $\nu_2=0.75$ ), respectively.

smaller, the grafting site gets close to the adsorbing surface, and then the side chain easily can adsorb (and if it is long enough, the side chain adsorption will have a kind of feedback effect on the backbone, dragging the remaining part of the nonadsorbed loop toward the surface as well). Clearly, this picture is qualitative and somewhat speculative, but it

suggests that through a cooperative interplay of side chains and backbone, a much more intricate behavior is possible than for the adsorption of linear polymers. One can even speculate that due to the strong crowding effects upon adsorption, occurring especially for long side chains, a complete adsorption of the bottle-brush cannot occur from a con-

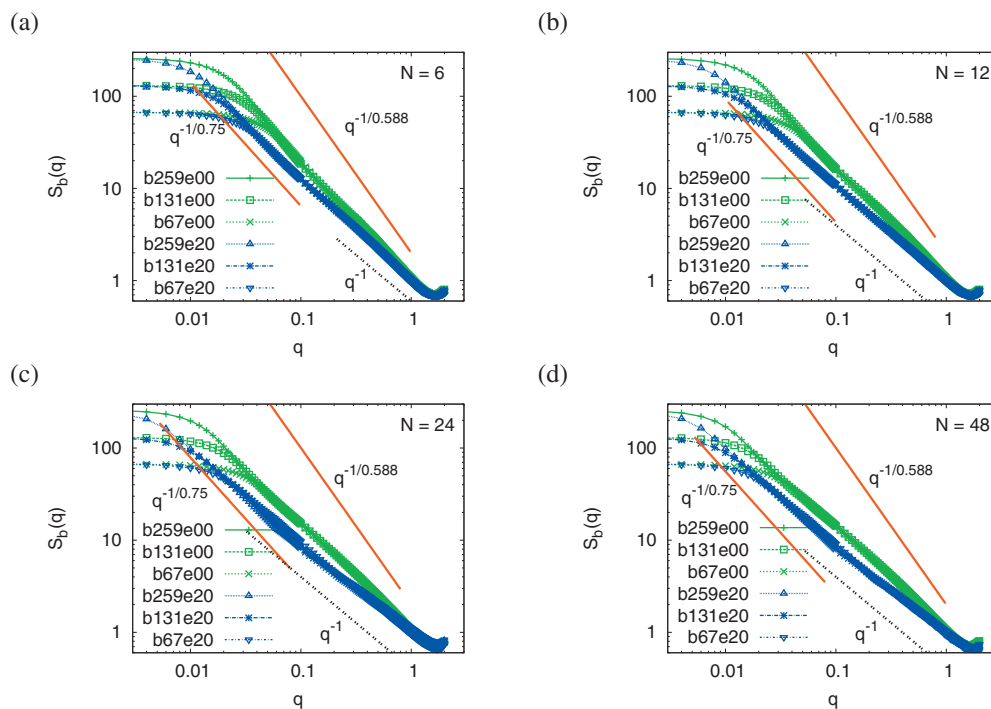


FIG. 17. Log-log plot of the scattering function  $S_b(q)$  of the monomers in the backbone vs wave number  $q$  for side chain lengths (a)  $N=6$ , (b)  $N=12$ , (c)  $N=24$ , and (d)  $N=48$ . Three choices of backbone chain lengths  $N_b=67$ , 131, and 259 are included in the same notation as in Fig. 16 is used.

figuration where both ends are already adsorbed and a train is still present in the interior of the polymer. Rather, the adsorbed part toward the free end of the backbone would have to desorb again first, and then the complete adsorption proceeds in a zipperlike fashion starting from the grafted chain end. Of course, the development of an analytical model that could describe data such as those shown in Figs. 2, 3, 9, and 15 would be highly desirable.

We have also verified that strongly adsorbed bottle-brush polymers exhibit lateral linear dimensions that scale with the exponent  $\nu_2$  of two-dimensional self-avoiding walks, and in the scattering function of the total bottle-brush, this behavior is seen as well (Fig. 16). However, the expected rodlike behavior on intermediate length scales is only seen when the scattering from the backbone is isolated (Fig. 17). Our data also imply rather different structures of adsorbed versus non-adsorbed bottle-brush polymers, making it difficult to reason from adsorbed structures on the behavior of free bottle-brushes in solution! We emphasize this simple point as a warning to premature interpretations of corresponding experiments.

Our study reveals many details [bimodal behavior of the density distribution  $P(z)$  of the monomers as a function of distance from the surface near adsorption (Fig. 13), characteristic effects due to the backbone chain ends (Figs. 5–8), etc.], which all reflect in some way the interplay between the enthalpy won by adsorbing monomers and various entropic effects. More work is clearly required to clarify the reasons for these detailed observations. Also, it would be very interesting to clarify the nature of the cross-sectional structure of the adsorbed bottle-brush on a coarse-grained scale (in the bulk, the bottle-brush can be viewed as a more or less flexible cylinder: should we view the cross section of an adsorbed bottle-brush as a sphere cap rather than a sphere?). A further interesting aspect is the question of the persistence length of adsorbed bottle-brushes<sup>41,42</sup> and its relation to the persistence length of bottle-brushes in the bulk. Other interesting issues concern the effect of solvent quality<sup>43</sup> and possible irreversibility effects on the adsorption of the side arms.<sup>44</sup> Our study only considers adsorption under very good solvent conditions. It is also a very interesting problem (and relevant for experiment) to consider adsorption under poor solvent conditions where much more compact pancake structures should result<sup>43</sup> rather than the configurations obtained here, which resemble two-dimensional self-avoiding walks. Finally, we mention the possibility that for strong adsorption ( $\epsilon \gg \epsilon_c$ ), the left-right distribution of the side chains with respect to the backbone is quenched, i.e., random fluctuations in this distribution have not enough time to relax. Such effects are predicted to have interesting effects on the conformation of such strongly adsorbed bottle-brush polymers.<sup>44</sup> We intend to study some of these issues in forthcoming work.

## ACKNOWLEDGMENTS

H.-P.H. received funding from the Deutsche Forschungsgemeinschaft (DFG) under Grant No. SFB 625/A3. We are

grateful for extensive grants of computer time at the JU-ROPA under Project No. HMZ03 and SOFTCOMP computers at the Jülich Supercomputing Centre (JSC).

## APPENDIX: SCALING ANALYSIS OF THE ADSORPTION TRANSITION BOTTLE-BRUSH POLYMERS

In the previous work where the adsorption transition of flexible chains end-grafted by a chain end on an impenetrable surface was studied by Monte Carlo methods,<sup>26,29,31,32</sup> the location of the transition in the limit of infinite number of bonds between the monomers,  $N_b \rightarrow \infty$ , typically has been extracted from a scaling analysis.<sup>26</sup> The statement of scaling is that quantities such as the fraction  $N_s/N_b$  of adsorbed monomers do not depend on the two variables  $N_b$ ,  $\kappa = (\epsilon - \epsilon_c)/\epsilon_c$  in the most general way, but are essentially a function of a simple scaling variable,  $\zeta = \kappa N_b^\phi$ , apart from a power law prefactor. Thus,

$$N_s = N_b^\phi F_s(\zeta), \quad \kappa \rightarrow 0, \quad N_b \rightarrow \infty. \quad (\text{A1})$$

The power laws quoted in the main text [Eq. (1)] simply result from Eq. (A1) for  $\zeta \rightarrow -\infty$ ,  $\zeta = 0$ , and  $\zeta \rightarrow +\infty$ . Similar scaling results hold for the linear dimensions of the chains, e.g., the mean square gyration radius components of the backbone of the bottle-brush perpendicular and parallel to the surface are

$$R_{gb,z}^2 = N_b^{2\nu} F_{bz}(\zeta), \quad R_{gb,\parallel}^2 = N_b^{2\nu} F_{b\parallel}(\zeta), \quad (\text{A2})$$

and again Eq. (A2) is supposed to be valid in the limit where both  $\kappa \rightarrow 0$  and  $N_b \rightarrow \infty$ . For Eq. (A2), the scaling functions for  $\zeta \leq 0$  are less interesting since  $F_{bz}(\zeta \rightarrow -\infty)$ ,  $F_{b\parallel}(\zeta \rightarrow -\infty)$ ,  $F_{bz}(0)$ , and  $F_{b\parallel}(0)$  are finite constants [cf. Eq. (2)]. However, for  $\zeta \rightarrow +\infty$ , one has

$$F_{bz}(\zeta) \propto \zeta^{-2\nu/\phi}, \quad F_{b\parallel}(\zeta) \propto \zeta^{2(\nu_2 - \nu)/\phi}, \quad (\text{A3})$$

and combining Eqs. (A2) and (A3), one hence recovers Eqs. (3) and (4) of the main text.

Of course, the singularities described by Eqs. (1)–(4) of the main text and the above Eqs. (A1)–(A3) emerge only in the double limit  $\kappa \rightarrow 0$ ,  $N_b \rightarrow \infty$ : for any finite  $N_b$  functions  $N_s(\epsilon)$ ,  $R_{gb,z}^2(\epsilon)$  and  $R_{gb,\parallel}^2(\epsilon)$  as regular functions of  $\epsilon$ , the singular behavior is rounded off, as is well known.<sup>26</sup> Thus, the estimation of  $\epsilon_c$  is a nontrivial matter. What usually is done (see, e.g. Refs. 26, 31, and 32) is a “data collapsing method”—one varies both  $\epsilon_c$  and the (originally unknown) value of the crossover exponent to obtain an optimal “data collapse” of the set of functions  $N_s(\epsilon, N_b)$ ,  $R_{gb,z}^2(\epsilon, N_b)$  and  $R_{gb,\parallel}^2(\epsilon, N_b)$  on these “master curves,” which represent then the three scaling functions  $F_s(\zeta)$ ,  $F_{bz}(\zeta)$ , and  $F_{b\parallel}(\zeta)$ . Figures 18–21 show some typical attempts to do this with our data [each figure has four parts to show the results for the four side chain lengths  $N=0$  (no side chains),  $N=6$ ,  $N=12$ , and  $N=24$ , respectively]. Here, we have used as a further constraint the “universality principle,” namely, the crossover exponent  $\phi$  should be a universal constant, independent of irrelevant microscopic details such as the length  $N$  of the side chains (as long as  $N$  is finite, while the limit  $N_b \rightarrow \infty$  is considered). Note also that the ratio  $R_{gb,z}^2/R_{gb,\parallel}^2$  according to

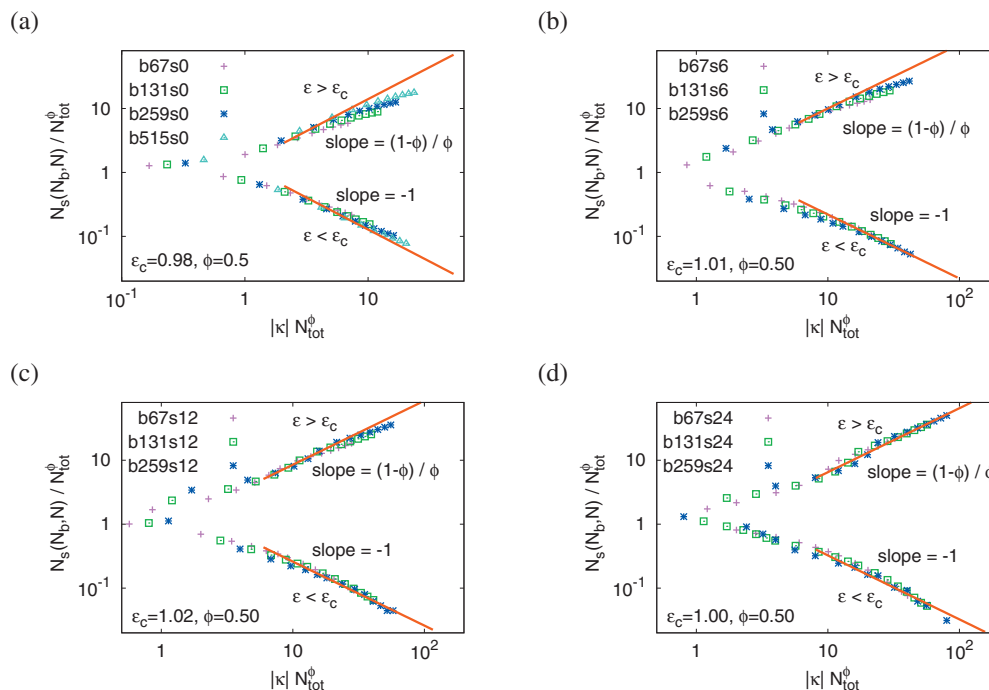


FIG. 18. Log-log plot of the rescaled surface contacts  $N_s/N_{\text{tot}}^\phi$  vs  $|\kappa|N_{\text{tot}}^\phi$  for  $\phi=0.50$ . Data for backbone lengths  $N_b=67, 131, 259$ , and  $515$  are included, as well as side chain lengths (a)  $N=0$ , (b)  $N=6$ , (c)  $N=12$ , and (d)  $N=24$ .

Eq. (A2) should be a function of  $\zeta$  alone and plotted versus  $\epsilon$  should have a unique intersection point at  $\epsilon_c$ . (However, as shown in Fig. 4, one would need data for larger  $N_b$  and very good statistical accuracy to show this).

The straight lines included in these log-log plots of the resulting estimates for the scaling functions that they must converge to for  $|\zeta| \rightarrow \infty$  yield the power laws quoted in Eqs. (1)–(4). Since  $\nu=0.588$  and  $\nu_2=3/4$  are independently known, it is again only the exponent  $\phi$  (as in the scaling

variable  $\kappa N_b^\phi$ ) that matters. To simplify matters, we only present the two extreme choices for  $\phi$  here: the estimate  $\phi=0.5$  (which happens to coincide with the crossover exponent for adsorption of Gaussian chains<sup>26–28</sup> but is supported by a renormalization group estimation<sup>30</sup> and some Monte Carlo studies<sup>29</sup>) and the most recent estimate  $\phi=0.59$  from Monte Carlo studies.<sup>32</sup> A comparison of Figs. 18 and 19 for  $N_s$  shows that we confirm the finding of Descas *et al.*,<sup>32</sup> that  $\phi=0.59$  yields a slightly better data collapse on the master

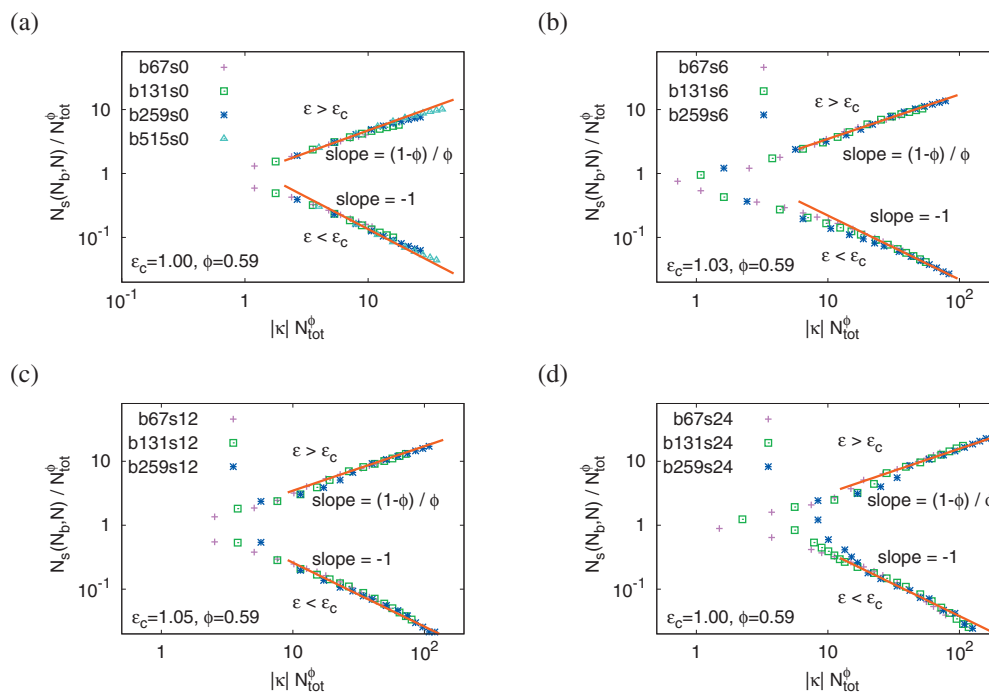


FIG. 19. Log-log plot of the rescaled surface contacts  $N_s/N_{\text{tot}}^\phi$  vs  $|\kappa|N_{\text{tot}}^\phi$  for  $\phi=0.59$ . Data for backbone lengths  $N_b=67, 131, 259$ , and  $515$  are included, as well as side chain lengths (a)  $N=0$ , (b)  $N=6$ , (c)  $N=12$ , and (d)  $N=24$ .

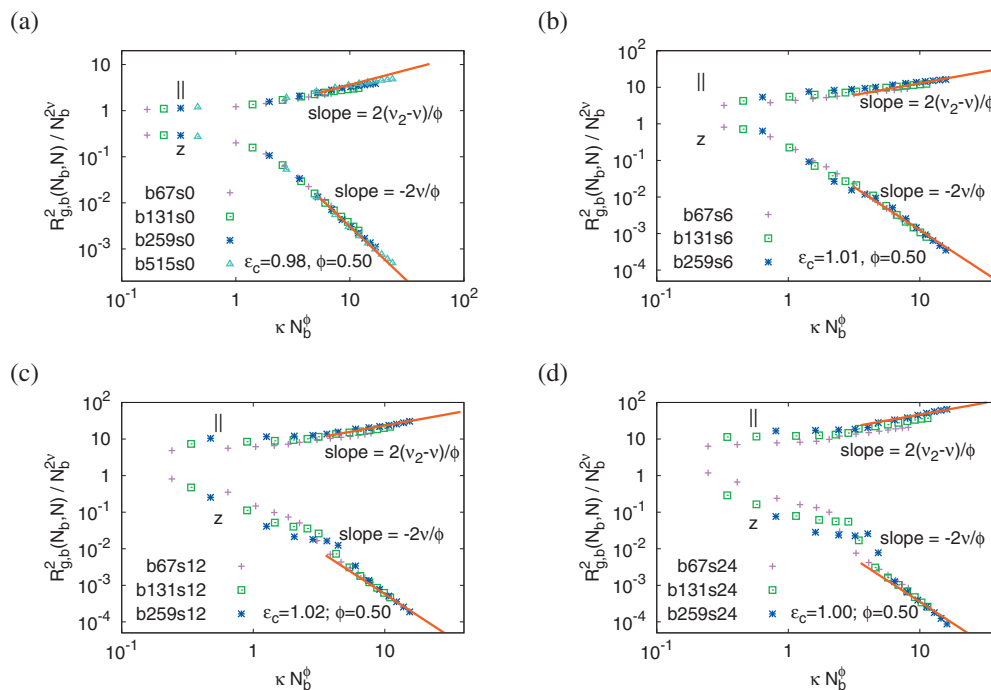


FIG. 20. Log-log plot of the mean square gyration radius components perpendicular and parallel to the surface,  $R_{g,b,z}^2/N_b^{2\nu}$  and  $R_{g,b,\parallel}^2/N_b^{2\nu}$ , respectively, vs  $\kappa N_b^\phi$  for  $\phi=0.50$ . Data for backbone lengths  $N_b=67, 131, 259$ , and  $515$  are included, as well as side chain lengths (a)  $N=0$ , (b)  $N=6$ , (c)  $N=12$ , and (d)  $N=24$ . Here, the Flory exponents  $\nu_2=3/4$  (2D) and  $\nu=0.588$  (3D).

curve  $F_s(\zeta)$ ,  $\epsilon_c(N)$  being always chosen such that for  $\epsilon < \epsilon_c$ , the master curve has the correct slope. For  $\epsilon > \epsilon_c$ , the data for large  $\zeta$  fall systematically somewhat below the expected power law if  $\phi=0.5$  is chosen. However, as a caveat, we mention that for finite  $N_b$ , the data are not expected to follow the master curve for very large  $\zeta$  since  $N_s/N_b \rightarrow 1$  (for the case  $N=0$  and large enough  $\epsilon$ , where the chain is adsorbed in

a two-dimensional configuration). So, it must happen that for large  $\zeta$ , the curves bend away from the power laws that describe the asymptotic limit of the scaling function, and this “saturation effect” occurs the later the larger  $N_b$  is, and this is exactly what one sees in Fig. 18(a), while in Fig. 19(a) the same effect is somewhat less pronounced. However, in our opinion, the evidence from these plots that  $\phi=0.59$  is “bet-

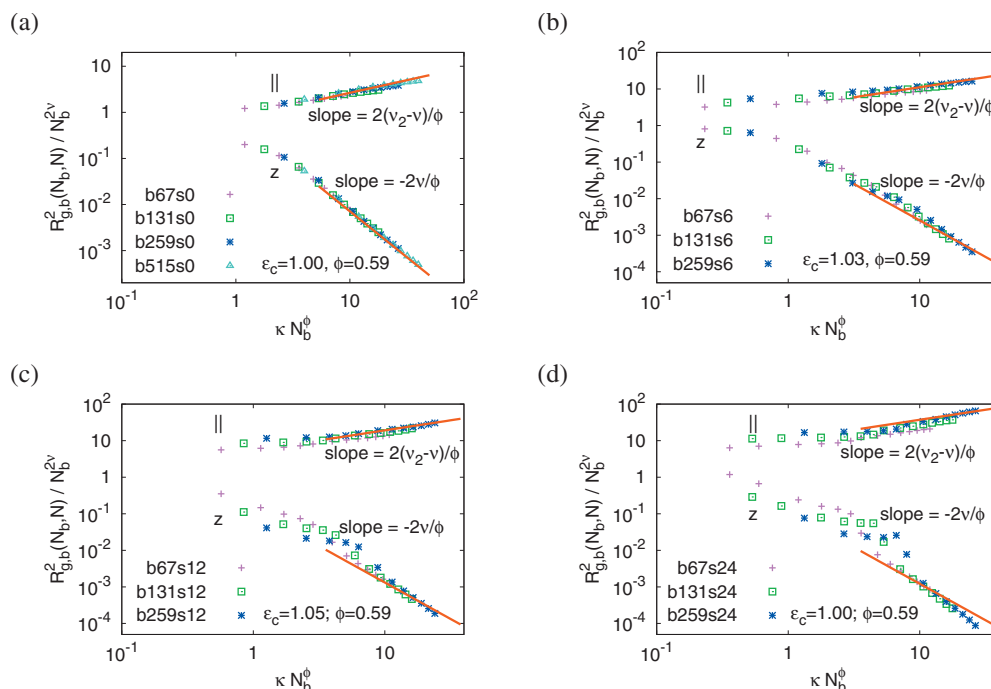


FIG. 21. Log-log plot of the mean square gyration radius components perpendicular and parallel to the surface,  $R_{g,b,z}^2/N_b^{2\nu}$  and  $R_{g,b,\parallel}^2/N_b^{2\nu}$ , respectively, vs  $\kappa N_b^\phi$  for  $\phi=0.59$ . Data for backbone lengths  $N_b=67, 131, 259$ , and  $515$  are included, as well as side chain lengths (a)  $N=0$ , (b)  $N=6$ , (c)  $N=12$ , and (d)  $N=24$ . Here, the Flory exponents  $\nu_2=3/4$  (2D), and  $\nu=0.588$  (3D).

ter" than  $\phi=0.50$  is somewhat weak, and much longer chains would be needed to reach a really firm conclusions.

When one chooses  $\phi=0.50$ , the resulting estimates for  $\epsilon_c(N)$  would be 0.98, 1.01, 1.02, and 1.00 for side chain lengths  $N=0, 6, 12$ , and  $24$ , respectively. When one chooses  $\phi=0.59$ , on the other hand, most of the estimates are a little bit larger, namely, 1.00, 1.03, 1.05, and 1.00, respectively. As expected, the best estimates for  $\phi$  and  $\epsilon_c(N)$  are correlated. However, it must be admitted that slightly different choices of  $\epsilon_c(N)$  than those that are shown here yield a data collapse that is only slightly worse. Given the fact that Eqs. (1)–(4) and (A1)–(A3) are only asymptotically valid in the double limit  $\kappa \rightarrow 0$  and  $N_b \rightarrow \infty$ , while for finite  $N_b$  and finite nonzero  $\kappa$ , corrections to scaling may be present, and a reliable judgment of accuracy for the estimates  $\epsilon_c(N)$  is difficult. For this reason, we have quoted  $\epsilon_c \approx 1.0$  as an estimate for all choices of  $N$  studied in the main text.

In fact, the estimation is not really improved when one considers the scaling of the mean square gyration radius (Figs. 20 and 21). For  $N=0$  and  $N=6$ , the quality of the data collapse for  $\phi=0.50$  and  $\phi=0.59$  is of comparable quality. For  $N=12$  and  $N=24$ , scaling seems to work well only for large  $\zeta$ , not for small  $\zeta$ , indicating clearly a more complex behavior right at the adsorption transition. The data show that the choices for  $\epsilon_c(N)$  quoted above are compatible with the behavior of the chain dimensions too, at least roughly.

The result that the addition of side chains (that are still short, of course) has so little effect on the location of the adsorption transition clearly is surprising and unexpected. Therefore, we have presented in this Appendix our evidence for this fact in some detail, notwithstanding the uncertainty about the best value of the crossover exponent; this problem is not solved by our analysis.

<sup>1</sup>M. Zhang and A. H. E. Müller, *J. Polym. Sci., Part A: Polym. Chem.* **43**, 3461 (2005).

<sup>2</sup>A. V. Subbotin and A. N. Semenov, *Polym. Sci., Ser. A* **49**, 1328 (2007).

<sup>3</sup>S. S. Sheiko, B. S. Sumerlin, and K. Matyjaszewski, *Prog. Polym. Sci.* **33**, 759 (2008).

<sup>4</sup>I. I. Potemkin and V. V. Palyulin, *Polym. Sci., Ser. A* **51**, 123 (2009).

<sup>5</sup>Y. Tsukahara, K. Mizuno, A. Segawa, and Y. Yamashita, *Macromolecules* **22**, 1546 (1989); Y. Tsukahara, K. Tsutsumi, Y. Yamashita, and S. Shimada, *ibid.* **23**, 5201 (1990).

<sup>6</sup>M. Wintermantel, M. Gerle, K. Fischer, M. Schmidt, I. Wataoka, H. Urakawa, K. Kajiwara, and Y. Tsukahara, *Macromolecules* **29**, 978 (1996).

<sup>7</sup>R. Djalali, S.-Y. Li, and M. Schmidt, *Macromolecules* **35**, 4282 (2002).

<sup>8</sup>T. Stephan, S. Muth, and M. Schmidt, *Macromolecules* **35**, 9857 (2002).

<sup>9</sup>C. Li, N. Gunari, K. Fischer, A. Janshoff, and M. Schmidt, *Angew. Chem., Int. Ed.* **43**, 1101 (2004).

<sup>10</sup>*Proteoglycans: Structure, Biology, and Molecular Interactions*, edited by

R. V. Iozzo (Dekker, New York, 2000).

<sup>11</sup>N. C. Kaneider, S. Duzendorfer, and C. J. Wiedermann, *Biochemistry* **43**, 237 (2004).

<sup>12</sup>J. Klein, *Science* **323**, 47 (2009).

<sup>13</sup>A. Sartori, A. Johner, J.-L. Viovy, and J.-F. Joanny, *Macromolecules* **38**, 3432 (2005).

<sup>14</sup>P. G. Khalatur, A. R. Khokhlov, S. A. Prokhorova, S. S. Sheiko, M. Möller, P. Reineker, D. G. Shirvanyanz, and N. Starovoitova, *Eur. Phys. J. E* **1**, 99 (2000).

<sup>15</sup>I. I. Potemkin, A. R. Khokhlov, S. Prokhorova, S. S. Sheiko, M. Möller, K. L. Beers, and K. Matyjaszewski, *Macromolecules* **37**, 3918 (2004).

<sup>16</sup>N. Gunari, M. Schmidt, and A. Janshoff, *Macromolecules* **39**, 2219 (2006).

<sup>17</sup>S. Rathgeber, T. Pakula, A. Wilk, K. Matyjaszewski, and K. L. Beers, *J. Chem. Phys.* **122**, 124904 (2005).

<sup>18</sup>B. Zhang, F. Gröhn, J. S. Pedersen, K. Fischer, and M. Schmidt, *Macromolecules* **39**, 8440 (2006).

<sup>19</sup>H.-P. Hsu, W. Paul, S. Rathgeber, and K. Binder, *Macromolecules* **43**, 1592 (2010).

<sup>20</sup>I. I. Potemkin, *Macromolecules* **39**, 7178 (2006).

<sup>21</sup>S. Elli, G. Raffaini, F. Ganazzoli, E. G. Timoshenko, and Y. A. Kuznetsov, *Polymer* **49**, 1716 (2008).

<sup>22</sup>P. G. de Gennes, *Scaling Concepts in Polymer Physics* (Cornell University Press, Ithaca, 1979).

<sup>23</sup>Note that previous work on the adsorption transition of comb polymers used  $N=5$  only (Ref. 21).

<sup>24</sup>P. G. De Gennes, *J. Phys. (Paris)* **37**, 1445 (1976).

<sup>25</sup>P. G. de Gennes, *Macromolecules* **13**, 1069 (1980).

<sup>26</sup>E. Eisenriegler, K. Kremer, and K. Binder, *J. Chem. Phys.* **77**, 6296 (1982).

<sup>27</sup>G. J. Fleer, M. A. Cohen-Stuart, J. M. H. M. Scheutjens, T. Cosgrove, and B. Vincent, *Polymers at Interfaces* (Chapman and Hall, London, 1993).

<sup>28</sup>E. Eisenriegler, *Polymers near Surfaces* (World Scientific, Singapore, 1993).

<sup>29</sup>R. Hegger and P. Grassberger, *J. Phys. A* **27**, 4069 (1994).

<sup>30</sup>H. W. Diehl and M. Shpot, *Nucl. Phys. B* **528**, 595 (1998).

<sup>31</sup>S. Metzger, M. Müller, K. Binder, and J. Baschnagel, *Macromol. Theory Simul.* **11**, 985 (2002); *J. Chem. Phys.* **118**, 8489 (2003).

<sup>32</sup>R. Descas, J.-U. Sommer, and A. Blumen, *Macromol. Theory Simul.* **17**, 429 (2008); *J. Chem. Phys.* **120**, 8831 (2004).

<sup>33</sup>V. A. Ivanov, J. A. Martemyanova, M. Müller, W. Paul, and K. Binder, *J. Phys. Chem. B* **113**, 3653 (2009).

<sup>34</sup>I. Carmesin and K. Kremer, *Macromolecules* **21**, 2819 (1988).

<sup>35</sup>H. P. Deutsch and K. Binder, *J. Chem. Phys.* **94**, 2294 (1991).

<sup>36</sup>W. Paul, K. Binder, D. W. Heermann, and K. Kremer, *J. Phys. II* **1**, 37 (1991).

<sup>37</sup>*Monte Carlo and Molecular Dynamics Simulations in Polymer Science*, edited by K. Binder (Oxford University Press, New York, 1995).

<sup>38</sup>H.-P. Hsu, W. Paul, and K. Binder, *Macromolecules* **43**, 3094 (2010).

<sup>39</sup>J. P. Wittmer, P. Beckrich, H. Meyer, A. Cavallo, A. Johner, and J. Baschnagel, *Phys. Rev. E* **76**, 011803 (2007).

<sup>40</sup>For a review, see A. D. Sokal in Ref. 37, p. 47.

<sup>41</sup>I. I. Potemkin and K. I. Popov, *J. Chem. Phys.* **129**, 124901 (2008).

<sup>42</sup>L. Feuz, F. A. M. Leermakers, M. Textor, and O. Borisov, *Macromolecules* **38**, 8891 (2005).

<sup>43</sup>M. O. Gallyamov, B. Tartsch, P. Mela, I. I. Potemkin, S. S. Sheiko, H. Börner, K. Matyjaszewski, A. R. Khokhlov, and M. Möller, *J. Polym. Sci., Part B: Polym. Phys.* **45**, 2368 (2007).

<sup>44</sup>I. I. Potemkin, *Macromolecules* **40**, 1238 (2007).